Breakdown of the velocity and turbulence in the wake of a wind turbine - Part 2: Analytical modeling.

Erwan Jézéquel[1,2], Frédéric Blondel[1], and Valéry Masson[2]

[1]IFP Energies nouvelles, 1-4 Avenue de Bois Préau, Rueil-Malmaison, France
[2]Centre National de Recherches Météorologiques, 42 avenue Gaspard Coriolis, Toulouse, France

Correspondence: Erwan Jézéquel (erwan.jezequel@ifpen.fr)

Abstract. This work aims at developing an analytical model for the velocity and turbulence in the wake of a wind turbine ~~that takes meandering into account and~~ where the expansion and the meandering of the wake can be independently calibrated. The velocity and turbulence ~~breakdown~~ breakdowns presented in the companion paper ~~allows~~ allow a better interpretation of the physical phenomena at stake and ~~facilitates~~ facilitate the modelling, in particular when it comes to wakes in a non-neutral atmosphere. A model for the dominating terms of these breakdowns is here proposed, using only five input parameters: the widths (in vertical and horizontal directions) of the non-meandering wake, the standard deviation of wake meandering (in both directions) and a mixing length. This model can be used either in the FFOR for a static approach or in the MFOR combined with the dynamic wake meandering model for an unsteady approach. The resulting shapes are tested on a neutral and an unstable LES dataset that was computed with Meso-NH. The model shows good results for the axial velocity in both directions. For the axial turbulence, the horizontal profiles are satisfying but further research is needed on the treatment of shear and the parametrisation of the missing terms to better reproduce the vertical asymmetry.

1 Introduction

The CPU cost of classical computational fluid dynamic models is too ~~large~~ high to deal with all the different cases needed to estimate and optimise the performances of a wind farm. Thus, so-called engineering models have been developed to estimate the power loss due to wakes at a low computational cost, e.g. Jensen (1983); Frandsen et al. (2006); Larsen et al. (2008); Bastankhah and Porté-Agel (2014). These design tools are based on physical considerations and are often calibrated and validated against numerical results or measurements. Among these tools, analytical models are the simplest: they consist of a single formula that can be directly applied to the wind farm setup and atmospheric conditions, leading to fast results even for a whole farm. A very commonly used model is the one developed by Bastankhah and Porté-Agel (2014) who assumed an axisymmetric and self-similar Gaussian velocity deficit in the wake and solved the mass and momentum conservation equations to find a relation between the amplitude and width of the Gaussian. It can be adapted for a non-axisymmetric wake (Xie and Archer, 2014):

$$\Delta U(x,y,z) = \frac{\overline{U}_\infty - \overline{U}}{\overline{U}_\infty} = C(x)\exp\left(-\frac{y^2}{2\sigma_y(x)^2} - \frac{z^2}{2\sigma_z(x)^2}\right) \tag{1}$$

$$C(x) = 1 - \sqrt{1 - \frac{C_T}{8\sigma_y(x)\sigma_z(x)/D^2}} \tag{2}$$

where $\overline{U}$ is the mean velocity field, $\overline{U}_\infty$ is the mean velocity upstream of the turbine, $C(x)$ is the maximum velocity deficit, C_T is the thrust coefficient, D is the turbine diameter, (x,y,z) are the streamwise, lateral and vertical coordinates, centred at the turbine's hub, and $\sigma_{y,z}$ the wake widths in the lateral and vertical directions. In this work, the vertical and horizontal axes are centred at the hub position. Here and in the following, the Reynolds decomposition is used to write any unsteady field $X(t)$ as a sum of a mean and a varying part: $X(t) = \overline{X} + X'(t)$. For the turbulent kinetic energy (TKE), ~~the IEC 61400-1 standard focuses on the maximum turbulence level in the wake,~~ it is common to model only the maximum value of added turbulence which can be ~~deduced by the~~ computed with the Crespo model (Crespo and Hernandez, 1996) or the Frandsen model (Frandsen, 2007) ~~using only the thrust coefficient and the downstream distance. More elaborated models exist where the whole profile is described, but are empirical (Ishihara and Qian, 2018).~~ as in the IEC 61400-1 standard. Their approach is mainly empirical and can be extended to describe the whole profile of turbulence instead of the maximum value alone (Ishihara and Qian, 2018). More recently, a physically-based model for each Reynolds' stress component has been proposed based on self-similarity (Stein and Kaltenbach, 2019).

The stability of the atmospheric boundary layer (ABL) influences the wake recovery (Abkar and Porté-Agel, 2015) and the large-scale eddies carried in this region of the atmosphere are often associated with wake meandering, i.e. oscillations of the instantaneous wake around its mean position (Larsen et al., 2008). To model the meandering, the concepts of fixed and moving frames of reference (respectively denoted FFOR and MFOR) defined in the dynamic wake meandering (DWM) model are used herein. The FFOR is bound to the ground: it is the frame of reference in which we want to compute the turbulence and velocity fields. In the FFOR the effects of meandering are not differentiated from the wake expansion ~~due~~ caused to turbulent mixing, making the fields in ~~the~~ this frame of reference harder to interpret. The MFOR is moving with the wake centre at each time step: in this frame of reference, only the wake expansion due to turbulent mixing is represented. The instantaneous streamwise velocity can be changed from one frame to another according to the relation:

$$U_{MF}(x,y,z,t) = U_{FF}(x, y + y_c(x,t), z + z_c(x,t), t) \tag{3}$$

where subscripts MF and FF denote the velocity fields in the MFOR and FFOR respectively, $y_c(x,t)$ and $z_c(x,t)$ are the time series of the wake centre's coordinates at the downstream position x. The concept of MFOR and FFOR can be used to write an analytical wake model for the velocity deficit as in the work Braunbehrens and Segalini (2019):

$$\Delta U(y,z) = C\left[1 + \left(\frac{\sigma_{fy}}{\sigma_y}\right)\right]^{-1/2}\left[1 + \left(\frac{\sigma_{fz}}{\sigma_z}\right)\right]^{-1/2}\exp\left[-\frac{y^2}{2\sigma_y^2 + 2\sigma_{fy}^2} - \frac{z^2}{2\sigma_z^2 + 2\sigma_{fz}^2}\right] \tag{4}$$

where $\sigma_{fy,fz}(x)$ are the standard deviations of the wake centre~~position~~ 's coordinates in the lateral and vertical directions respectively, $\sigma_{y,z}(x)$ are the wake widths in the MFOR and $C(x)$ is the maximum velocity deficit in the MFOR. Such a model allows calibrating independently the effects of meandering (through the variables $\sigma_{fy,fz}$) and of wake expansion due to turbulent mixing (through the variables $\sigma_{y,z}$). The former parameters are a function of atmospheric stability through lateral and vertical turbulence (Braunbehrens and Segalini, 2019; Du et al., 2021; Brugger et al., 2022) whereas the latter parameters can be a function of axial turbulence as in Eq. 1 (Fuertes et al., 2018; Niayifar and Porté-Agel, 2016) or turbine operating conditions such as C_T and atmospheric shear (Braunbehrens and Segalini, 2019).

The notation ~~$\widehat{U}_{MF} = U_{FF}$~~ $\widehat{a(y,z)} = a(y - y_c(t), z - z_c(t))$ for any field a, introduced in the companion paper, is used to shorten Eq. 3. For this work, it is also important to note that for any field a:

$$\overline{\widehat{a}} = \overline{a} * * f_c \tag{5}$$

where $**$ denotes a 2D convolution and f_c is the probability density function (PDF) of the wake centre position. In the companion paper, it has been shown that the velocity (Eq. 6) and turbulence (Eq. 7) in the FFOR can be expressed as a function of their counterparts in the MFOR. This is achieved by decomposing these quantities into several terms, noted (I) and (II) in Eq. 6 and (III) to (VII) in Eq. 7. ~~In~~

$$\overline{U_{FF}} = \underbrace{\overline{\widehat{U_{MF}}}}_{(I)} + \underbrace{\overline{\widehat{U'_{MF}}}}_{(II)} \tag{6}$$

$$k_{FF} = \underbrace{\overline{\widehat{U_{MF}}^2} - \overline{\widehat{U_{MF}}}^2}_{k_m=(III)} + \underbrace{\overline{\widehat{k_{MF}}}}_{k_a=(IV)} + \underbrace{2\mathrm{cov}\left(\widehat{U_{MF}}, \widehat{U'_{MF}}\right)}_{(V)} + \underbrace{\overline{\left(\widehat{U'^2_{MF}}\right)'}}_{(VI)} \underbrace{- \overline{\widehat{U'_{MF}}}^2}_{(VII)} \tag{7}$$

These terms are thoroughly described and quantified in the companion paper ~~, the magnitudes of these different terms have been compared, showing in particular~~ where they are separated into pure-terms ((I),(III) and (IV)) and cross-terms ((II), (V), (VI) and (VII)).

The term (I) is the convolution of $\overline{U_{MF}}$ with f_c. It is a pure mean velocity term: it is null only if the mean velocity is null. Conversely, the term (II) is a cross-term because it can be equal to 0 either if there is no meandering ($\widehat{x} = x$) or if there is no turbulence in the MFOR ($U'_{MF} = 0$). The term (III), also written k_m in the following to be consistent with notation from Keck et al. (2013) and Conti et al. (2021), is the turbulence purely induced by meandering: in the case of a meandering steady wake i.e. $U'_{MF} = 0$, Eq. 7 reduces to this term only. The term (IV) is the rotor added turbulence, which is also written k_a for consistency with other works. It is the turbulence purely induced by the rotor: in absence of meandering ($\widehat{x} = x$), the equation reduces to this term only, also written k_a in the following for consistency with the literature. Term (V) is the covariance of $\widehat{U_{MF}}$ and $\widehat{U'_{MF}}$, term (VI) can be viewed as the varying part of the MFOR turbulence and term (VII) is the square of the term (II). It

is a pure dissipation term as it is always negative. Like the term (II), they are cross-terms since they are equal to zero if either the turbulence in the MFOR or the meandering is null. The companion paper showed that terms (II) and (VII) are negligible in their respective equations. In the breakdown of the turbulence equation, terms (V) and (VI) are of lesser importance than (III) and (IV) but drive the vertical asymmetry of the turbulence profiles.

$$\overline{U_{FF}} = \underbrace{\overline{\widehat{U_{MF}}}}_{(I)} + \underbrace{\overline{\widehat{U'_{MF}}}}_{(II)}$$

$$k_{FF} = \underbrace{\overline{\widehat{U_{MF}}^2} - \overline{\widehat{U_{MF}}}^2}_{k_m=(III)} + \underbrace{\overline{\widehat{k_{MF}}}}_{k_a=(IV)} + \underbrace{2\mathrm{cov}\left(\widehat{U_{MF}}, \widehat{U'_{MF}}\right)}_{(V)} + \underbrace{\overline{\left(\widehat{U'^2_{MF}}\right)'}}_{(VI)} \underbrace{- \overline{\widehat{U'_{MF}}}^2}_{(VII)}$$

The objective of this paper is to propose an analytical model based on the velocity and turbulence breakdowns (Eqs. 6 and 7). Similarly to Eq. 4 (Braunbehrens and Segalini, 2019), the reasoning starts by writing the wake properties in the MFOR and the wake meandering with different parameters ~~in order~~ to take into account meandering due to atmospheric stability independently of the expansion due to turbulence mixing. ~~In the~~ It is common in wake modelling to assume that meandering can be entirely accounted for by increasing the wake expansion. In the present model, these phenomena are modelled separately, but it will be assumed that they do not interact. This is equivalent to neglecting cross-terms in Eqs. 6 and 7 which have been shown to take consistently smaller values than pure-terms in the companion paper. In the future though, modelling these cross-terms might be necessary to improve the results.

In the first section of this work, the reference datasets obtained from the large eddy simulations (LESs) used in the companion paper are described. The second section presents the assumptions of the model and the shape functions chosen for the meandering, velocity deficit and added turbulence in the MFOR. The third and fourth sections are dedicated to the results of the model for the velocity and turbulence fields, respectively. We will show that due to meandering, the turbulence in the wake no longer respects self-similarity and that another parameter is needed to yield correct shape functions in the wake.

2 The LESs datasets

The analytical model developed in this work is based on LESs datasets generated with the Meso-NH solver (Lac et al., 2018). It is a finite volume research code for ABL simulations where the Navier-Stokes equations and the energy conservation equation are resolved on an Arakawa C-grid. This solver models the stability of the ABL with a buoyancy term in the momentum equation. The Coriolis force and ~~large scale~~ large-scale forcing are also taken into account. The effect of the wind turbine on the surrounding flow is modelled with an actuator line method, i.e. rotating source terms in the momentum equation.

To close the set of equations, the subgrid TKE equation is resolved, allowing to write all the subgrid quantities as a function of this subgrid TKE, the resolved variables and a Deardorff mixing length. A grid nesting method allows having simultaneously

a vertical and horizontal mesh size of 0.5 m in the wake region and a domain large enough to compute the largest eddies of the atmosphere. The model and numerical parameters are described in more detail in the companion paper.

The simulated turbine is a modified version of the Vestas V27: it is a three-bladed rotor with a diameter $D = 27$ m and a hub height of 32.1 m. In the companion paper, three cases of stability were simulated but ~~since the model presented herein does not take veer into account, the~~ the stable case has been discarded for this paper ~~.~~ due to its strong veer. The veer could have been modelled as in Abkar et al. (2018) but it would significantly complicate the present derivations. Moreover, meandering and meandering turbulence are negligible in a stably stratified ABL (see companion paper) and thus there is little interest in using the approach presented herein. For the remaining neutral and unstable cases, the veer upstream of the turbine is negligible: respectively, the difference between the maximum and minimum wind direction between the ground and 90 m above the ground is of $1.25°$ and $0.5°$. The stability parameter at $z = 10$ m is respectively $z/L_{MO} = \{0.003, -0.16\}$ where L_{MO} is the Monin-Obukhov length, the inflow velocity at hub height is $U_h = \{8.4, 6.2\}$ m s^{-1}, the inflow streamwise turbulence intensity (TI) at hub height is $TI_x = \{11.2, 12.3\}$ %, the thrust coefficient is $C_T = \{0.79, 0.81\}$ and the rotational velocity of the turbine is fixed to $\Omega = \{4.56, 3.89\}$ rad s^{-1}. In this study, the wake is studied at eight positions downstream, from $x/D = 1$ to $x/D = 8$

The wake centre's coordinates $y_c(x,t)$ and $z_c(x,t)$ are computed at each time step and each downstream position with the *Constant Flux* wake tracking algorithm, ~~that~~ which is described in the companion paper. ~~In order to~~ To facilitate the wake tracking and to have cleaner results of velocity deficit and added turbulence in the MFOR, a *Reference* simulation is also run. It is a simulation with the same inflow and boundary conditions but without the wind turbine. ~~This~~ The corresponding velocity field noted U_{ref} is thus representing a developing ABL without the perturbations of a wind turbine. Even though there is no wake and thus no wake meandering, an equivalent MFOR can be deduced for this simulation by applying Eq. 3, with the y_c and z_c computed in the case with the wind turbine.

Due to limited computational resources for the post-processing, the LESs datasets are sampled at 1 Hz and do not take into account the subgrid turbulence. The resulting computations of TKE consequently do not take into account the variations at higher frequencies than this sampling frequency. Finally, only the mean streamwise velocity ($\overline{U}_x$), and the streamwise turbulence ($k_x = \overline{u'u'}$) are computed.

3 Independent modelling of the wake in the MFOR and meandering

An analytical form for some of the main terms of Eqs. 6 and 7 is proposed and tested on the neutral and unstable cases. ~~The stable case is not used since the presented model does not take veer into account, but such modification could be applied, following Abkar et al. (2018).~~ Similarly to what has been done in the companion paper, the normalised root-mean-square-error (RMSE, defined in Eq. 8) is used here to quantify the error between the model and the Meso-NH simulations. The reference value α is the value of the studied quantity in Meso-NH, α_p is the value predicted by the model and N is the number of samples, i.e. the number of mesh points in the studied 2D plane.

$$\text{RMSE} = \sqrt{\frac{\sum_{i=1}^{N}(\alpha - \alpha_p)^2}{N}}/(\alpha_{max} - \alpha_{min}) \tag{8}$$

3.1 Wake velocity deficit in the MFOR

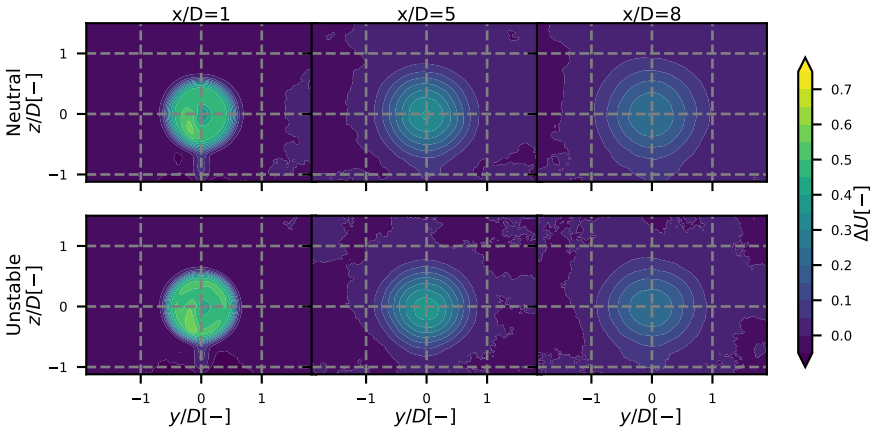

Figure 1. Velocity deficit in the MFOR for the neutral (top) and unstable (bottom) cases computed with Meso-NH.

The first step of this analytical reasoning is to define the shape of the mean velocity deficit and added turbulence fields in the MFOR. The velocity deficit ΔU in the MFOR computed from the reference dataset is plotted in Fig. 1 for the neutral and unstable cases at three positions downstream. In the LESs datasets, the velocity deficit in the MFOR is computed as:

$$\Delta U_{MF}(x,y,z) = \frac{\overline{U}_{x,MF,ref}(x,y,z) - \overline{U}_{x,MF}(x,y,z)}{\overline{U}_{x,MF,ref}(x,y,z)} \tag{9}$$

whereas in the analytical model, it is defined as:

$$\Delta U_{MF,am}(x,y,z) = \frac{U_{x,\infty}(z) - U_{x,MF,am}(x,y,z)}{U_{x,\infty}(z)} \tag{10}$$

where $U_{x,\infty}(z)$ (hereafter abbreviated $U_\infty(z)$) is the time-averaged and ~~laterally averaged~~ laterally-averaged streamwise velocity profile upstream the turbine. Equation 9 is used because it allows computing a smooth and almost axisymmetric velocity deficit in the MFOR, which is moreover very similar between the neutral and unstable cases. ~~However~~Even though it is convenient for the post-process of LES data, $\overline{U}_{x,MF,ref}$ ~~has no real physical and will not be modelled analytically, so it is natural to use~~ does not correspond to any physical reality so instead, Eq. 10 is used for the model. Based on the shapes observed in Fig. 1, this mean velocity deficit is modelled with the long-established Gaussian velocity deficit (cf Eq. 1):

$$\Delta U_{MF,am}(x,y,z) = C(x)\exp\left(-\frac{y^2}{2\sigma_y^2(x)} - \frac{z^2}{2\sigma_z^2(x)}\right) \tag{11}$$

where subscript $._{am}$ stands for "analytical model", $C(x)$ is defined in Eq. 2 and σ_y, σ_z are the wake widths in the MFOR, which are deduced from the LESs datasets (see Sect. 3.4). For both cases, the resulting velocity deficit is plotted in Fig. 2. The RMSE is higher in the near-wake because the shape of the velocity deficit is assumed to be Gaussian, whereas a "top-hat" function is observed in the LESs datasets. In the literature, it has been shown that double-Gaussian (Keane et al., 2016) or super-Gaussian (Blondel and Cathelain, 2020) shapes provide more accurate results, but here the Gaussian shape allows a straight-forward ~~computations~~ computation of our model and is still pertinent in the far wake for both datasets, especially in the unstable case.

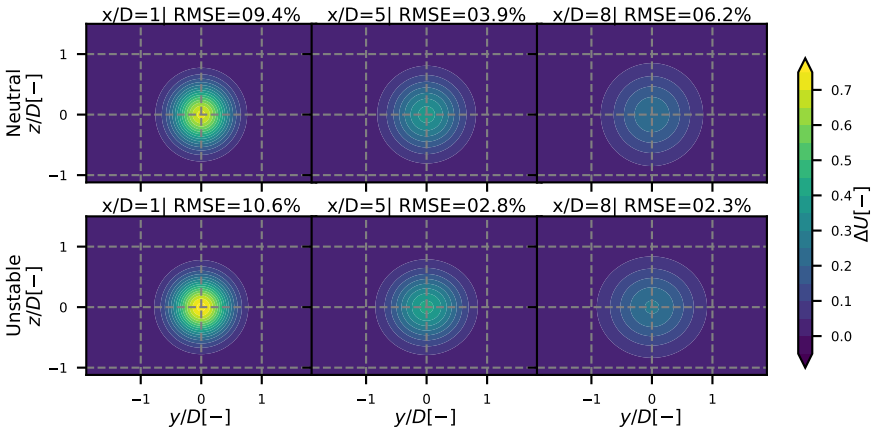

Figure 2. Modelled velocity deficit in the MFOR for the neutral (top) and unstable (bottom). The RMSE is given with respect to the LES value (Fig. 1).

3.2 Wake added turbulence in the MFOR

~~In order to~~ To model term (IV) or k_a, one needs an analytical form for the turbulence in the MFOR k_{MF}. It is proposed to separate the rotor-added turbulence Δ(IV) from the ambient turbulence. Similarly to the velocity deficit, the ambient turbulence is chosen as the value from the reference simulation for the LES dataset:

$$k_{x,MF}(x,y,z) = \Delta k_{x,MF}(x,y,z) + k_{x,MF,ref}(x,y,z) \tag{12}$$

but as the upstream value for the analytical model:

$$k_{x,MF,am}(x,y,z) = \Delta k_{x,MF,am}(x,y,z) + k_{x,\infty}(z) \tag{13}$$

where $\Delta k_{x,MF}$ ~~will be referred hereafter as "added turbulence"~~ is the added streamwise turbulence in the MFOR and $k_{x,\infty}$ (abbreviated k_∞) is the laterally averaged streamwise turbulence upstream of the turbine. The added axial turbulence field in the MFOR computed from the LESs datasets is plotted in Fig. 3. It is normalised like a turbulence intensity to have similar orders of magnitude between the neutral and unstable datasets:

$$\Delta TI_{MF} = \frac{|\Delta k_{x,MF}|}{\Delta k_{x,MF}} \cdot \frac{\sqrt{|\Delta k_{x,MF}|}}{U_h} \tag{14}$$

where U_h is the upstream velocity at hub height. Similarly to the velocity deficit, the added turbulence field in the MFOR is very ~~similar~~ alike between the two cases of stability~~, indicating that the turbulence added by the rotor depends more on the operating conditions (C_T, tip-speed ratio) than on the atmospheric conditions (velocity at hub height, atmospheric stability. ..). The only atmospheric parameter that seems to influence ΔTI_{MF} is the shear (in particular in~~ . Atmospheric stability and hub-height velocity are thus not parameters of the added turbulence in the MFOR, as long as sufficiently large turbulent structures are present in the inflow (Jézéquel et al., 2022). Instead, shear has a clear effect in the neutral case~~), which breaks~~ , by breaking the symmetry of the wake as it travels downstream. Other parameters, such as thrust coefficient or roughness length, may impact ΔTI_{MF} but are here constant among the two cases so more work is needed to estimate their impact.

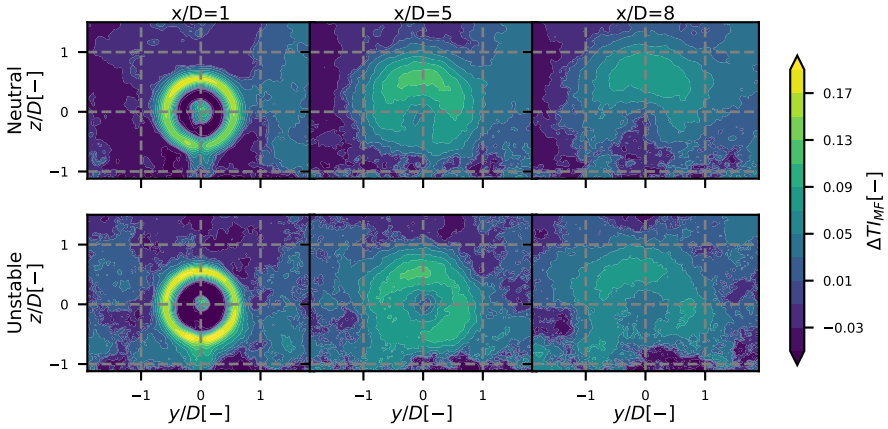

Figure 3. Added turbulence in the MFOR for the neutral (top) and unstable (bottom) case computed with Meso-NH.

The derivation of a model for $\Delta k_{x,MF}$ is not as straightforward as for ΔU_{MF} because turbulence comes from the unsteadiness of the flow whereas an analytical model is by definition steady. In the DWM, the Madsen formulation (Madsen et al., 2010) is used to scale the velocity profile with an empirical function of the wake-generated shear. One could also assume self-similarity of the $\Delta k_{x,MF}$ function and try to derive a model as it was done for the velocity in Bastankhah and Porté-Agel (2014). The main issue here is that an analytical form of the model is needed in the FFOR, i.e. the convolution of $f_{c,am}$ with the chosen shape function for $\Delta k_{x,MF,am}$ must have an analytical solution, which is not trivial for the aforementioned models.

It is here proposed to assume that the turbulence in the MFOR is solely driven by wake-generated shear. ~~In order to~~ To relate the turbulence in the MFOR to mean gradients, two models for the velocity scale u_0 are combined. In the first, it is assumed to be proportional to the square root of the TKE ~~k (Pope, 2000): $u_0 = C_\mu^{1/4} k^{1/2}$ where C_μ is a constant and l_m the mixing length~~(Pope, 2000). However in the present work, the three-dimensional TKE ~~k~~ is not computed, so it is replaced with the axial turbulence k_x:

$$u_0 = C_\mu^{1/4} k_x^{1/2}. \tag{15}$$

where C_μ is a constant and l_m is the mixing length. The value $C_\mu = 0.09$ will be used in this work. Note that this value has been fitted ~~in order~~ to yield correct behaviour in the log-law region of a wall, and can be extended in regions where the turbulence production equals the dissipation (Pope, 2000). It is a strong assumption that has not been verified, but since the mixing length is here fitted on the LES results, this choice has no significant consequences. In the future, it would be interesting to compute this constant in the MFOR of a wind turbine wake. In the second method, the velocity scale is defined from the norm of the strain-rate tensor $|\overline{\overline{S}}|$:

$$\begin{aligned} u_0 &= l_m |\overline{\overline{S}}| \\ &= l_m \cdot \sqrt{\left(\frac{\partial U_x}{\partial x}\right)^2 + \left(\frac{\partial U_y}{\partial y}\right)^2 + \left(\frac{\partial U_z}{\partial z}\right)^2 + \frac{1}{2}\left(\frac{\partial U_x}{\partial y} + \frac{\partial U_y}{\partial x}\right)^2 + \frac{1}{2}\left(\frac{\partial U_x}{\partial z} + \frac{\partial U_z}{\partial x}\right)^2 + \frac{1}{2}\left(\frac{\partial U_y}{\partial z} + \frac{\partial U_z}{\partial y}\right)^2} \end{aligned} \tag{16}$$

From the literature (Iungo et al., 2017), it appears that in the wake of a wind turbine, the dominating term (in cylindrical coordinates) is $\frac{\partial U}{\partial r}$. It is supposed herein that these results can be transposed in Cartesian coordinates and are ~~still viable~~ applicable in the MFOR. The velocity scale can thus be written as a function of the derivatives of the axial velocity.

$$u_0 = l_m \cdot \sqrt{\frac{1}{2}\left(\frac{\partial U_x}{\partial y}\right)^2 + \frac{1}{2}\left(\frac{\partial U_x}{\partial z}\right)^2} \tag{17}$$

To simplify the equation of added turbulence in the MFOR and to analytically develop the convolution product, it is needed to consider U_∞ as a constant with z when it comes to the vertical derivative, i.e. make the following approximation:

$$\frac{\partial U_x(y,z)}{\partial z} = U_\infty(z) \frac{\partial \Delta U(y,z)}{\partial z}. \tag{18}$$

Note that the model could be computed in the MFOR by developing the derivative with $U_x(y,z) = U_\infty(z)(1 + \Delta U(y,z))$ but then no analytical solution can be found for the rotor-added turbulence in the FFOR $\Delta k_{x,a,am}$ (i.e. after the convolution), either with a power law or a logarithmic profile for U_∞.

$$
\begin{aligned}
\Delta k_{x,MF,am} &= \left(\frac{u_0}{C_\mu^{1/4}}\right)^2 \\
&= \frac{l_m^2(x)}{2C_\mu^{1/2}} \cdot \left[\left(\frac{\partial U_{x,MF}}{\partial y}\right)^2 + \left(\frac{\partial U_{x,MF}}{\partial z}\right)^2\right] \\
&= \frac{(C(x)U_\infty(z)l_m(x))^2}{2C_\mu^{1/2}} \left[\left(\frac{\partial \Delta U_{MF,am}}{\partial y}\right)^2 + \left(\frac{\partial \Delta U_{MF,am}}{\partial z}\right)^2\right] \\
&= K_{MF}(x,z) \left[\left(\frac{y}{\sigma_y^2(x)}\right)^2 + \left(\frac{z}{\sigma_z^2(x)}\right)^2\right] e^{-\frac{y^2}{\sigma_y^2(x)} - \frac{z^2}{\sigma_z^2(x)}} \exp\left(-\frac{y^2}{\sigma_y^2(x)} - \frac{z^2}{\sigma_z^2(x)}\right)
\end{aligned}
\tag{19}
$$

Computing the mixing length in Eq. 19 is a challenge that has not been answered yet in this work. Formulations that depend on the vertical coordinate (like the Prandtl mixing length $l_m = \kappa z$ or the modified version of **?**) are not appropriate herein because they would result in a value constant with x whereas the work of Iungo et al. (2017) showed the opposite in a wind turbine wake. Local formulations such as **?** could also be used but would increase the complexity of the model and for this particular case would lead to the simplification of $k_{x,MF,am}$, which we want to avoid since it is the variable of interest. Moreover, these formulations have been developed for the ABL whereas we are looking for a mixing length to apply to the wake in the MFOR, which is relatively independent of the ABL state (Jézéquel et al., 2021).

It has thus been decided to use a mixing length that only depends on the streamwise direction $l_m(x)$. Two mixing length values proposed in the literature have been tried (Keck et al., 2012; Iungo et al., 2017) without success. However, the authors think that these type of formulations are more appropriate than those aforementioned but need some modifications to fit our model. A proper formulation of the mixing length will be proposed in further works, but for the present work, the value of l_m at each position downstream is deduced through an optimisation algorithm (see Sect. 3.4).

The maps of $\Delta k_{x,MF,am}$, normalised as in Eq. 14 (in order to compare with Fig. 3) are plotted in Fig. 4. Strong assumptions were made to obtain Eq. 19, especially on shear, which led to an almost axisymmetric turbulence field in the MFOR. Indeed, the only component inducing vertical asymmetry in Eq. 19 is $U_\infty(z)^2$. In the neutral case, the ratio between the squared velocity at top and bottom tip is $U_\infty^2(z = +D/2)/U_\infty^2(z = -D/2) \approx 1.2$, a fairly low value compared to e.g. Fig. 3 at $x/D = 5$ where the ratio of added turbulence at these positions is about 2.

Moreover, the error in the near-wake due to the Gaussian shape assumption for velocity deficit in the MFOR propagates onto $\Delta k_{x,MF,am}$, leading to a much weaker but more spread axial turbulence. Note that the RMSE are significantly higher than for ΔU_{MF}. Finally, the model imposes that $\Delta k_{x,MF,am} = 0$ at the centre of the wake, a condition that is not fulfilled in the reference dataset (Fig. 3). A possible improvement would be to add the streamwise gradient $\partial U_x/\partial x$ in Eq. 17. Despite these flaws, this expression has been chosen since it has an analytical solution of its convolution with the wake centre position distribution $f_{c,am}$ and gives acceptable results. Note that an empirical correction can be used to correct for the overestimation in the near wake (Ishihara and Qian, 2018), but this option has not been retained in the presented work since it aimed to build a fully physically-built model.

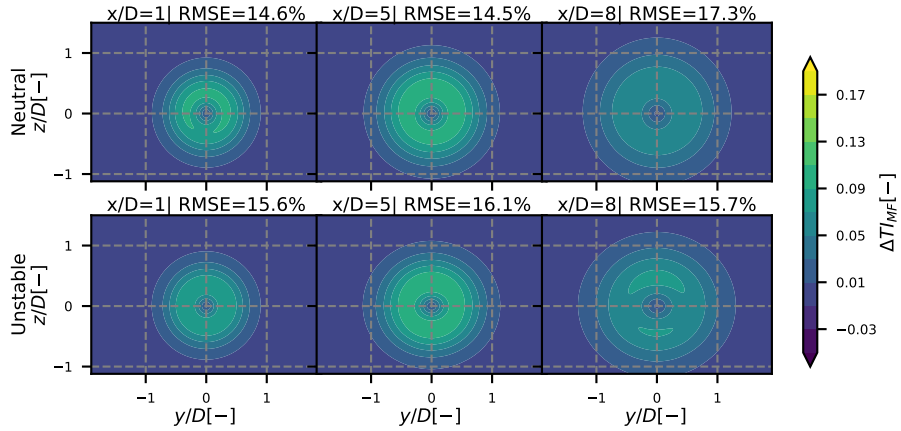

Figure 4. Modelled added turbulence in the MFOR. The RMSE is given with respect to the s values in Fig. 3.

3.3 Wake meandering

For the PDF of wake meandering, the central limit theorem leads to a Gaussian distribution (Braunbehrens and Segalini, 2019):

$$f_{c,am}(x,y,z) = \frac{1}{2\pi\sigma_{fy}(x)\sigma_{fz}(x)}\exp\left(-\frac{y^2}{2\sigma_{fy}^2(x)} - \frac{z^2}{2\sigma_{fz}^2(x)}\right) \tag{20}$$

The distribution of the wake centre f_c is known to be non-axisymmetric and thus its ~~distribution~~ variance σ_f is defined in both dimensions. In Fig. 5, the partial distributions $f_{cy} = 1/(\sqrt{2\pi}\sigma_{fy})\exp(-y^2/(2\sigma_{fy}^2))$ and $f_{cz} = 1/(\sqrt{2\pi}\sigma_{fz})\exp(-z^2/(2\sigma_{fz}^2))$ are plotted against the histograms of $y_c(t)$ and $z_c(t)$ found in the LESs datasets. The RMSE computed between the 2D histograms and Eq. 20 is indicated at each downstream position (the first value corresponds to the neutral case and the second to the unstable case). It appears that the results are much better in the neutral case (in ~~green~~orange) than in the unstable case (in red). This is likely due to the higher meandering in the unstable case, which would require a higher number of data to reach a converged PDF, whereas it has twice less data as the neutral case (see the companion paper for more details). Simulations of more than 40 minutes should thus be performed ~~in order~~ to have a converged meandering distribution for such atmospheric stability and rotor size. Moreover, in the vertical direction, the shape of the LES histogram is closer to a skewed Gaussian than a symmetric Gaussian shape due to the ground presence.

The RMSE associated to $\Delta U_{MF,am}$, $\Delta k_{x,MF,am}$ and $f_{c,am}$ (respectively Figs 2, 4 and 5) indicate the sources of error from the different assumptions. For the velocity model that uses only $\Delta U_{MF,am}$ and $f_{c,am}$, the error will come from the Gaussian shape hypothesis of the velocity deficit in the near wake and from the Gaussian distribution of the wake centre in the far wake. For the turbulence model that uses the three functions, the error will come mainly from the chosen function of $\Delta k_{a,MF,am}$, in particular for the neutral case, due to the bad accounting of shear.

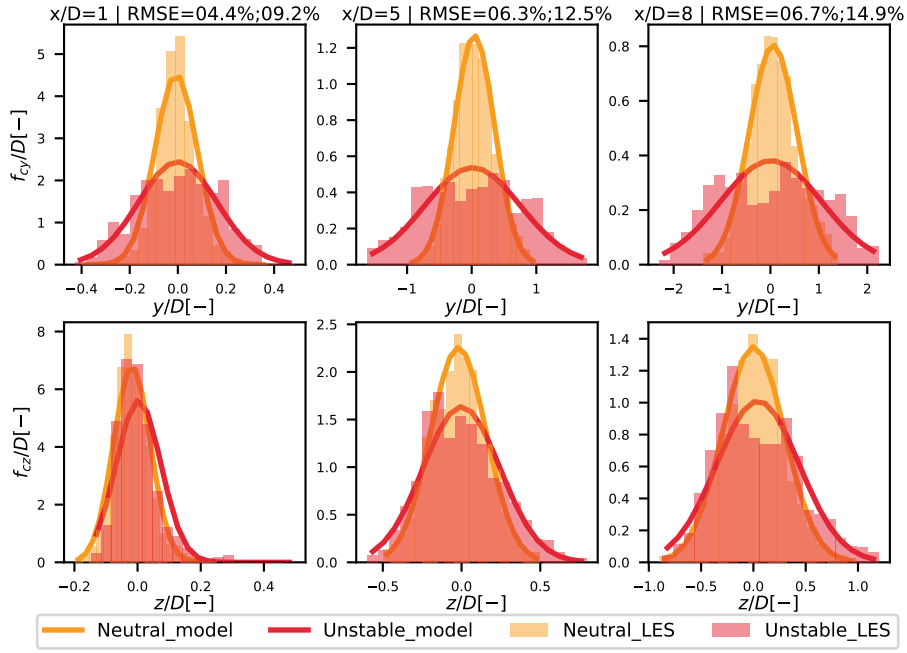

Figure 5. Histograms of the wake distribution in Meso-NH along with the modelled distributions (solid lines), in the horizontal (top) and vertical (bottom) directions. The RMSE is computed in the YZ plane.

3.4 Computation of the model's parameters

In the following, the dependency of the variables on coordinates x is omitted to lighten the equations. The presented work does not aim at calibrating properly the modelled terms but simply to show that a simple shape function can already lead to a rather good approximation. Consequently, the parameters that should normally be calibrated as a function of the turbine operating conditions and atmospheric states are here directly deduced from the LES field:

- The widths of the wake in the MFOR (σ_y, σ_z) are deduced from fitting the function of Eq. 21 on the velocity deficit ~~ΔU~~ΔU_{MF} through a non-linear least squares method.

$$f(y,z,C_0,y_0,z_0,\sigma_y,\sigma_z,\omega) = C_0 + C\exp\left(-a(y-y_0)^2 - 2b(y-y_0)(z-z_0) - c(z-z_0)^2\right) \tag{21}$$

with $a = \left(\frac{cos^2\omega}{2\sigma_y^2} + \frac{sin^2\omega}{2\sigma_z^2}\right)$, $b = \left(-\frac{sin2\omega}{4\sigma_y^2} + \frac{sin2\omega}{4\sigma_z^2}\right)$ and $c = \left(\frac{sin^2\omega}{2\sigma_y^2} + \frac{cos^2\omega}{2\sigma_z^2}\right)$. Parameter C is fixed as in Eq. 2, and the optimisation is run on parameters $\{C_0, y_0, z_0, \sigma_y, \sigma_z, \omega\}$ where ω is the angle of rotation of the wake, y_0, z_0 the mean wake deviation, and C_0 and offset to help the algorithm.

– The widths of the wake centre distribution σ_{fy} and σ_{fz} are computed as the variances of the wake centre's coordinate $y_c(x,t)$ and $z_c(x,t)$:

$$\sigma_{fy}(x) = \sqrt{\overline{y_c(x,t)'^2}}\,; \quad \sigma_{fz}(x) = \sqrt{\overline{z_c(x,t)'^2}} \tag{22}$$

– The mixing length $l_m(x)$ is imposed so that Eq. 19 fits the streamwise turbulence in the MFOR (see Fig. 3) ~~.~~ at each position x. This optimisation is done with a non-linear least squares method.

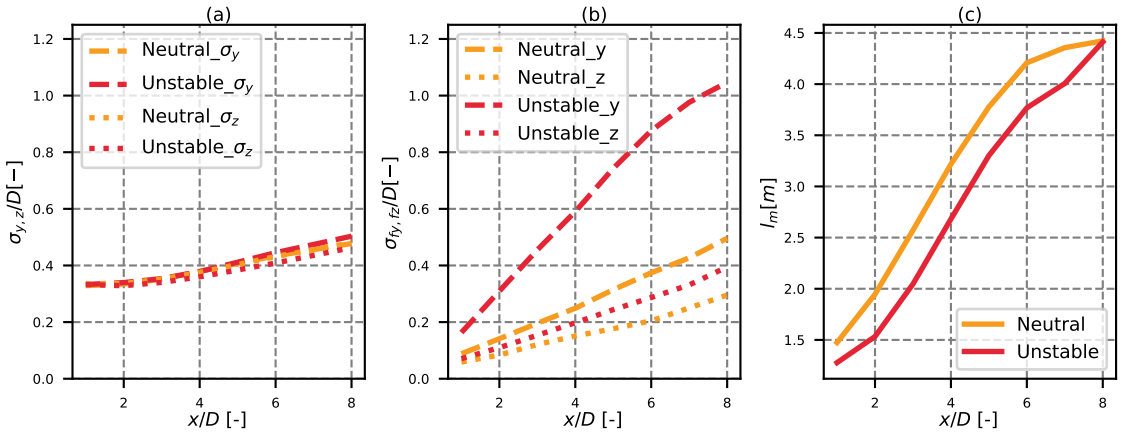

Figure 6. Wake properties calibrated from the neutral and unstable cases: (a) wake width in the MFOR; (b) wake meandering; (c) mixing length.

The resulting values for σ_y, σ_z, σ_{fy}, σ_{fz} and l_m are plotted as a function of the downstream direction x/D in Fig. 6 and are also used to plot Figs. 2, 5 and 4. The unstable and neutral wake widths in the MFOR are close to each other and the wake is approximately ~~axisymmetric~~ describing a circle i.e. $\sigma_y = \sigma_z$. It is however not necessarily axisymmetric due to the shear. Conversely, the amount of meandering is much higher in the unstable case compared to the neutral case and in the horizontal direction compared to the vertical direction. ~~In the MFOR, the wake is almost axisymmetric (if the atmospheric shear is neglected): the fact that wakes are more elongated~~ Thus, the fact that in the FFOR, wakes are wider in the horizontal than the vertical direction ~~in the FFOR~~ and in an unstable ABL compared to a neutral ABL mostly comes from the meandering. ~~From Figs. 6a and 6b, it is seen that the amount of meandering starts lower but grows faster than the wake width, in particular in the unstable case. Consequently, the total wake width in the FFOR $\sigma_{ty,tz} = \sqrt{\sigma_{y,z}^2 + \sigma_{fy,fz}^2}$ (see Eq. 25) will be close to σ for $x \to 0$ and if the meandering is sufficiently strong, it will be close to σ_f as $x \to \infty$.~~ This observation underlines the pertinence of our approach to differentiate meandering from wake expansion. Finally, the mixing length plotted in Fig. 6c shows an approximately linear behaviour between $x/D = 2$ and $x/D = 6$, followed by a break of the slope. It is difficult to conclude for this relatively small range of x but it is reassuring that the shape is similar to Iungo et al. (2017). Moreover, this linear behaviour will be convenient to model in the future.

4 Model for the velocity in the FFOR

In Eq. 6, the velocity in the wake is written under its dimensional form whereas the model chosen in Eq. 11 is written under the velocity deficit form. ~~In order to~~ To relate the velocity to the velocity deficit, it is needed to assume that despite its dependency on z ~~(due to shear)~~due to the atmospheric shear, the upstream velocity U_∞ can be considered as a constant when applying the 2D convolution product with the wake centre distribution. For any function $g(y,z)$, this simplification can be written:

$$f_{c,am}(y,z) **(U_\infty(z)\cdot g(y,z)) = U_\infty(z)\cdot[f_{c,am}(y,z) ** g(y,z)]\,. \tag{23}$$

An analytical form of the term (I) can then be deduced from ~~the~~ Eqs. 11 and 20:

$$\begin{aligned} U_{x,FF,am}(y,z) &= f_{c,am}(y,z) ** [U_\infty(z)\,(1+\Delta U_{FF,am}(y,z))] \\ &= U_\infty(z)\left(1+\int\int \Delta U_{MF,am}(y-y_c,z-z_c)\cdot f_{c,am}(y_c,z_c)dy_c dz_c\right) \\ &= U_\infty(z)\,(1+\Delta U_{FF,am}) \end{aligned} \tag{24}$$

The velocity deficit in the FFOR $\Delta U_{FF,am}$ is thus the convolution product of two Gaussian functions. It is known that the convolution product of two normalised Gaussian functions of variance σ_a^2 and σ_b^2 is a normalised Gaussian function of variance $\sigma_a^2+\sigma_b^2$ (Teitelbaum). Equation 24 can be written as the product of two convolution products, leading to:

$$\begin{aligned} \Delta U_{FF,am} &= 2C\pi\sigma_y\sigma_z\left[\int \frac{1}{\sqrt{2\pi}\sigma_y}\exp\left(-\frac{(y-y_c)^2}{2\sigma_y^2}\right)\frac{1}{\sqrt{2\pi}\sigma_{fy}}\exp\left(-\frac{y_c^2}{2\sigma_{fy}^2}\right)dy_c\right. \\ &\qquad \left.\int \frac{1}{\sqrt{2\pi}\sigma_z}\exp\left(-\frac{(z-z_c)^2}{2\sigma_z^2}\right)\frac{1}{\sqrt{2\pi}\sigma_{fz}}\exp\left(-\frac{z_c^2}{2\sigma_{fz}^2}\right)dz_c\right] \\ &= C\sqrt{\frac{\sigma_y^2}{\sigma_y^2+\sigma_{fy}^2}\frac{\sigma_z^2}{\sigma_z^2+\sigma_{fz}^2}}\exp\left(-\frac{y^2}{2\sigma_y^2+2\sigma_{fy}^2}-\frac{z^2}{2\sigma_z^2+2\sigma_{fz}^2}\right) \end{aligned} \tag{25}$$

Even though the reasoning of Braunbehrens and Segalini (2019) is different, it is here shown that their model (Eq. 4) can be found by neglecting term (II) and assuming Eq. 23 as well as Gaussian shapes for the velocity deficit in the MFOR and the wake centre's distribution. This is still a Gaussian form i.e. Eq. 1 with a FFOR wake widths defined as $\sigma_{ty,tz}=\sqrt{\sigma_{y,z}^2+\sigma_{fy,fz}^2}$, and a maximum velocity deficit of:

$$C_{FF} = C\sqrt{\frac{\sigma_y^2}{\sigma_y^2+\sigma_{fy}^2}\frac{\sigma_z^2}{\sigma_z^2+\sigma_{fz}^2}}. \tag{26}$$

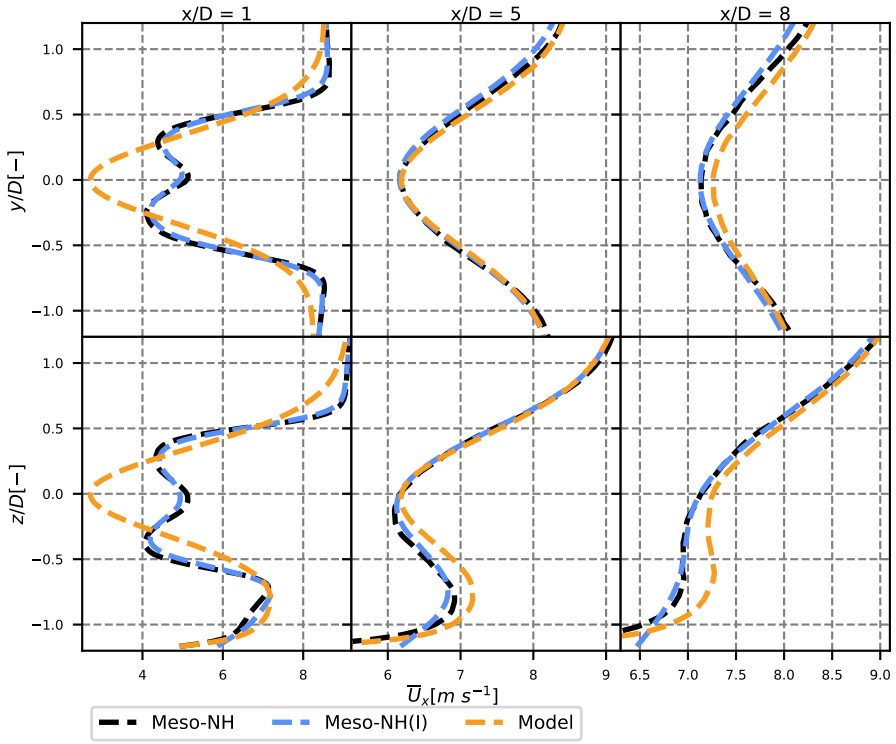

Figure 7. Results of the analytical velocity model (orange) in the neutral case, compared to the modelled term in Meso-NH (blue) and the total velocity in the FFOR (black) for the neutral case. Lateral (top) and vertical (bottom) profiles are plotted for different positions downstream.

From Figs. 6a and 6b, the amount of meandering starts lower but grows faster than the wake width, in particular in the unstable case. Hence, one can expect that $\sigma_{ty,tz}$ will be close to σ for $x \to 0$ and if the meandering is sufficiently strong, it will be close to σ_f as $x \to \infty$.

$$C_{FF} = C\sqrt{\frac{\sigma_y^2}{\sigma_y^2+\sigma_{fy}^2}\frac{\sigma_z^2}{\sigma_z^2+\sigma_{fz}^2}}.$$

To fulfill the conservation of momentum as in Eq. 2, one would need $C_{FF} = 1-\sqrt{1-C_T/(8\sigma_{ty}\sigma_{tz}/D^2)}$, which is not the case here. Actually, with this methodology, the conservation of momentum can only be enforced in the MFOR or ~~in~~ the FFOR. This is the consequence of neglecting the term (II) in the velocity breakdown, however, the error hence induced is relatively low (not shown here). Combining Eqs. 24 and 25 leads to our model for the velocity in the wake of a wind turbine:

$$U_{x,FF,am}(y,z) = U_\infty(z)\left(1+C\sqrt{\frac{\sigma_y^2}{\sigma_y^2+\sigma_{fy}^2}\frac{\sigma_z^2}{\sigma_z^2+\sigma_{fz}^2}}\exp\left(-\frac{y^2}{2\sigma_y^2+2\sigma_{fy}^2}-\frac{z^2}{2\sigma_z^2+2\sigma_{fz}^2}\right)\right) \quad (27)$$

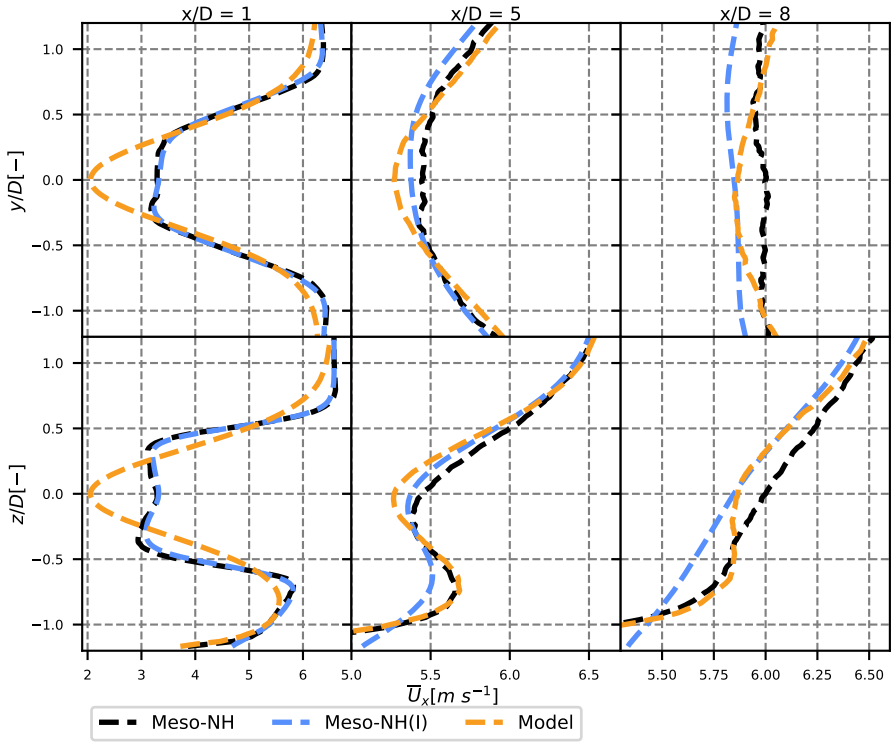

Figure 8. Results of the analytical velocity model (orange) in the unstable case, compared to the modelled term in Meso-NH (blue) and the total velocity in the FFOR (black) for the unstable case. Lateral (top) and vertical (bottom) profiles are plotted for different positions downstream.

The resulting horizontal (top) and vertical (bottom) velocity profiles computed with the parameters from Fig. 6a and 6b are plotted in Figs. 7 and 8 for the neutral and unstable cases, respectively. On the same figures are also plotted the velocity profiles in the FFOR in Meso-NH and the velocity profiles of the term (I) computed in Meso-NH, which is the only term modelled in the velocity breakdown equation. Despite the error in the near wake, the shapes are well-reproduced as soon as the wake takes an actual Gaussian shape. In the neutral case, the fit is good, except near the ground, where the assumption on shear (Eq. 23) might be too constraining. These overall good results confirm that the ~~hypothesis~~ hypotheses made in Sect. 3 for the velocity in the MFOR and the wake centre distribution are good and that meandering has been correctly computed.

~~Results of the analytical velocity model (orange) in the unstable case, compared to the modelled term in Meso-NH (blue) and the total velocity in the FFOR (black) for the unstable case. Lateral (top) and vertical (bottom) profiles are plotted for different positions downstream.~~

In the unstable case (Fig. 8), the results are still good but some discrepancies are observed with the reference data. As pointed out in Sect. 3, the error on $f_{c,am}$ is larger in the unstable case than in the neutral case, supposedly because the unstable simulation has not run for long enough. Moreover, the tracking might not have been as good as in the neutral case: if all the movements due to meandering have not been detected by the tracking algorithm, the computed σ_{fz} is underestimated,

explaining why the Gaussian shape is more pronounced in the model than in the reference data. Finally, the term (II) takes larger relative values ~~in~~ for this case, explaining the larger gap between the blue and black curves in Fig. 8 compared to Fig. 7. Since the analytical model is a model of the term (I) i.e. the blue curve, it increases the potential error compared to the actual velocity field in the FFOR (black curve).

5 Model for the turbulence in the FFOR

5.1 Meandering term

With the same assumptions as for the term (I), it is possible to derive an analytical formulation for the term (III) of Eq. 7 i.e. the turbulence induced by meandering. This meandering turbulence field computed with the two LESs datasets is plotted in Fig. 9 under its turbulence intensity value (see Eq. 14).

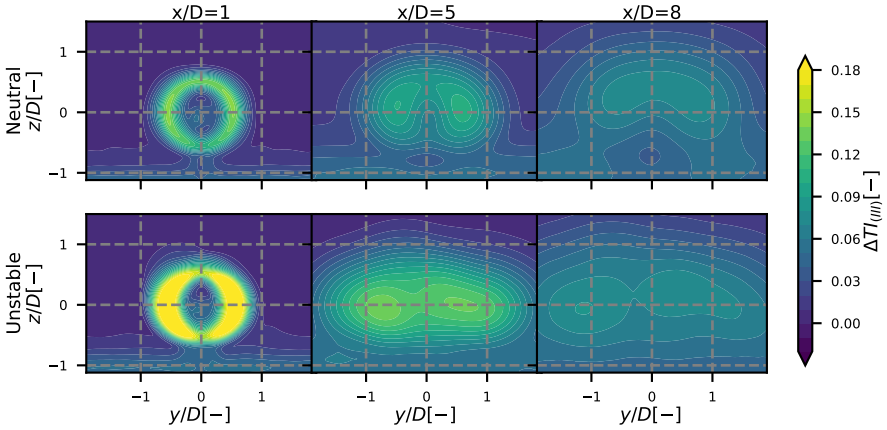

Figure 9. Meso-NH values of $k_{x,m}$ i.e. the term (III) for the neutral and unstable cases.

The assumption of Eq. 23 must again be used to get U_∞^2 out of the convolution product and Eq. 25 is reused to compute the right hand side of term (III): $\widehat{\overline{U_{MF}}}^2$. In the left hand side, there is a convolution of the Gaussian function $f_{c,am}$ with $\Delta U^2_{MF,am}$, which is also a Gaussian function of widths $\sqrt{0.5}\sigma_y$ and $\sqrt{0.5}\sigma_z$. It is thus possible to use the fact that the convolution of two Gaussian functions is a Gaussian function (Teitelbaum).

$$
\begin{aligned}
k_{x,m,am}(y,z) &= \left[f_{c,am} * * U^2_{x,MF,am}\right] - U^2_{x,FF,am} \\
&= U^2_\infty(z) \int\int \left(1 + \Delta U_{MF,am}(y - y_c, z - z_c)\right)^2 f_{c,am}(y_c, z_c) dy_c dz_c - U^2_\infty(z) \left(1 + \Delta U_{FF,am}\right)^2 \\
&= U^2_\infty(z) \int\int \Delta U^2_{MF,am}(y - y_c, z - z_c) f_{c,am}(y_c, z_c) dy_c dz_c - U^2_\infty(z) \Delta U^2_{FF,am} \\
&= (C U_\infty(z))^2 \left[\sqrt{\frac{\sigma_y^2}{\sigma_y^2 + 2\sigma_{fy}^2}} \sqrt{\frac{\sigma_z^2}{\sigma_z^2 + 2\sigma_{fz}^2}} \exp\left(-\frac{y^2}{\sigma_y^2 + 2\sigma_{fy}^2} - \frac{z^2}{\sigma_z^2 + 2\sigma_{fz}^2} \right) \right. \\
&\qquad \left. - \frac{\sigma_y^2}{\sigma_y^2 + \sigma_{fy}^2} \frac{\sigma_z^2}{\sigma_z^2 + \sigma_{fz}^2} \exp\left(-\frac{y^2}{\sigma_y^2 + \sigma_{fy}^2} - \frac{z^2}{\sigma_z^2 + \sigma_{fz}^2} \right) \right]
\end{aligned}
\tag{28}
$$

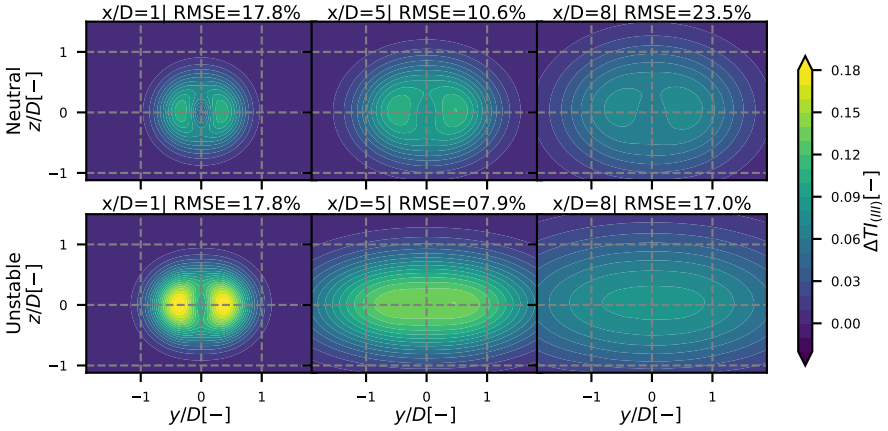

Figure 10. Results of $k_{x,m,am}$ i.e. the model for the term (III) for the neutral and unstable cases. The RMSE is given with respect to the term (III) computed from Meso-NH (Fig. 9).

The shape of term (III) is thus not a double Gaussian, as one could interpret from Fig. 9, but rather Gaussian of width $\sqrt{0.5\sigma^2 + \sigma_f^2}$ minus a thinner and less pronounced Gaussian of width $\sqrt{0.5\sigma^2 + 0.5\sigma_f^2}$. It can be verified that this expression is always larger than 0 i.e. the meandering only produces turbulence and does not dissipate it. The results of this model with the parameters shown in Figs. 6a and 6b is plotted in Fig. 10 at three positions downstream. To quantify the error induced by the model, the RMSE is computed between the model and the term (III) in the LESs datasets (Fig. 9). The results are overall promising: the shape and order of magnitude are respected for both cases. The increased error in the near and far wake is the direct consequence of the error made by the model on the term (I) and on the meandering estimation (see the two previous sections).

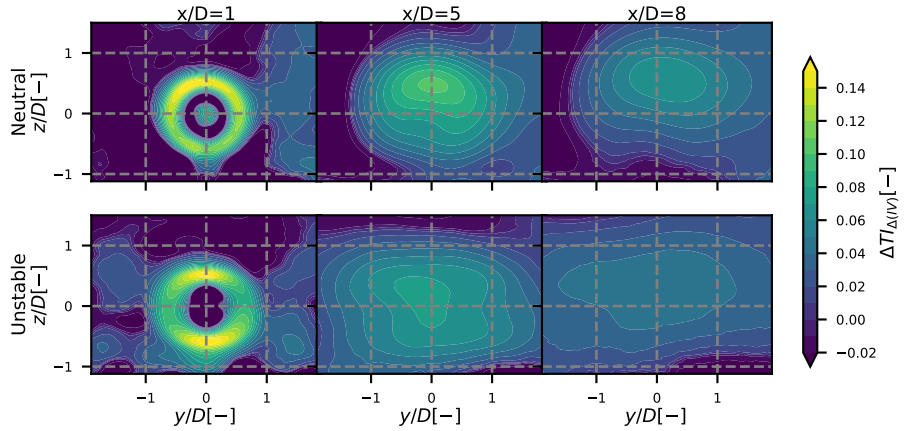

Figure 11. Results of the LESs datasets for term $\Delta k_{x,a}$ i.e. Δ(IV) for the neutral and unstable cases.

5.2 Rotor-added turbulence term

The term (IV) of Eq. 7, also written k_a for "rotor-added turbulence", is simply the 2D convolution of k_{MF} with f_c. However, it has been chosen to model $\Delta k_{x,MF,am} = k_{x,MF,am} - k_\infty$ instead of directly $k_{x,MF,am}$ because it is easier to interpret and model. Similarly to the unperturbed velocity, the reference turbulence is not modelled, so it is assumed that $\widehat{k_\infty(z)} = k_\infty(z)$ despite the dependency of k_∞ on z. In term of ~~added-turbulence~~added turbulence, it thus writes:

$$\Delta k_{x,a,am} = \overline{\widehat{\Delta k_{x,MF,am}}} \tag{29}$$

Applying the assumed shape for the added turbulence in the MFOR in Eq. 19 leads to an analytical form of the axial rotor-added turbulence:

$$\begin{aligned}
\Delta k_{x,a,am} &= \Delta k_{x,MF,am} ** f_{c,am} \\
&= \frac{K_{MF}}{2\pi\sigma_{fy}\sigma_{fz}} \int\int \left[\left(\frac{y_c}{\sigma_y^2}\right)^2 + \left(\frac{z_c}{\sigma_z^2}\right)^2 \right] \exp\left(-\frac{y_c^2}{\sigma_y^2} - \frac{z_c^2}{\sigma_z^2}\right) \exp\left(-\frac{(y-y_c)^2}{2\sigma_{fy}^2} - \frac{(z-z_c)^2}{2\sigma_{fz}^2}\right) dy_c dz_c \\
&= \frac{K_{MF}}{2\pi\sigma_{fy}\sigma_{fz}} \left[\int \left(\frac{y_c}{\sigma_y^2}\right)^2 \exp\left(-\frac{y_c^2}{\sigma_y^2} - \frac{(y-y_c)^2}{2\sigma_{fy}^2}\right) dy_c \int \exp\left(-\frac{z_c^2}{\sigma_z^2} - \frac{(z-z_c)^2}{2\sigma_{fz}^2}\right) dz_c \right. \\
&\qquad \left. + \int \left(\frac{z_c}{\sigma_z^2}\right)^2 \exp\left(-\frac{z_c^2}{\sigma_z^2} - \frac{(z-z_c)^2}{2\sigma_{fz}^2}\right) dz_c \int \exp\left(-\frac{y_c^2}{\sigma_y^2} - \frac{(y-y_c)^2}{2\sigma_{fy}^2}\right) dy_c \right]
\end{aligned} \tag{30}$$

At this point, the added turbulence in the FFOR is the sum of two terms, that are identical if the coordinates y and z are swapped~~: solving one of these terms makes the solution for the other trivial~~. It is the product of two convolutions: the first of

$f : y \to y^2 \exp(-y^2/\sigma_y^2)$ with a Gaussian function and the second of two Gaussian functions. The first convolution product has been solved with a computer algebra tool (Scherfgen) and the other has already been solved in Eq. 28. It gives:

$$
\begin{aligned}
&\int \left(\frac{y_c}{\sigma_y^2}\right)^2 \exp\left(-\frac{y_c^2}{\sigma_y^2} - \frac{(y-y_c)^2}{2\sigma_{fy}^2}\right) dy_c \int \exp\left(-\frac{z_c^2}{\sigma_z^2} - \frac{(z-z_c)^2}{2\sigma_{fz}^2}\right) dz_c \\
=&\frac{\sqrt{2\pi}\sigma_{fy}(\sigma_y^2 y^2 + \sigma_{fy}^4\sigma_y^2 + 2\sigma_{fy}^4)}{\sigma_y(\sigma_y^2 + 2\sigma_{fy}^2)^{5/2}} \exp\left(-\frac{y^2}{\sigma_y^2+\sigma_{fy}^2}\right) \frac{\sqrt{2\pi}\sigma_{fz}\sigma_z}{\sqrt{\sigma_z^2+2\sigma_{fz}^2}} \exp\left(-\frac{z^2}{\sigma_z^2+2\sigma_{fz}^2}\right) \\
=&2\pi\sigma_{fy}\sigma_{fz}\frac{\sigma_y\sigma_z}{\sqrt{\sigma_y^2+2\sigma_{fy}^2}\sqrt{\sigma_z^2+2\sigma_{fz}^2}} \frac{(\sigma_y^2 y^2 + \sigma_{fy}^2\sigma_y^2 + 2\sigma_{fy}^4)}{\sigma_y^2(\sigma_y^2+2\sigma_{fy}^2)^2} \exp\left(-\frac{y^2}{\sigma_y^2+\sigma_{fy}^2} - \frac{z^2}{\sigma_z^2+2\sigma_{fz}^2}\right)
\end{aligned} \tag{31}
$$

From Eq. 31, it remains to add the same quantity with $y \leftarrow z$ and $z \leftarrow y$, factorise and simplify to deduce the model for Δk_a:

$$
\Delta k_{x,a,am} = K_{FF}\left(\frac{y^2\sigma_y^2 + \sigma_y^2\sigma_{fy}^2 + 2\sigma_{fy}^4}{\sigma_y^2(\sigma_y^2+2\sigma_{fy}^2)^2} + \frac{z^2\sigma_z^2 + \sigma_z^2\sigma_{fz}^2 + 2\sigma_{fz}^4}{\sigma_z^2(\sigma_z^2+2\sigma_{fz}^2)^2}\right) \exp\left(-\frac{y^2}{\sigma_y^2+2\sigma_{fy}^2} - \frac{z^2}{\sigma_z^2+2\sigma_{fz}^2}\right) \tag{32}
$$

with:

$$
K_{FF} = \frac{K_{MF}}{\sqrt{1+2(\sigma_{fy}/\sigma_y)^2}\sqrt{1+2(\sigma_{fz}/\sigma_z)^2}}. \tag{33}
$$

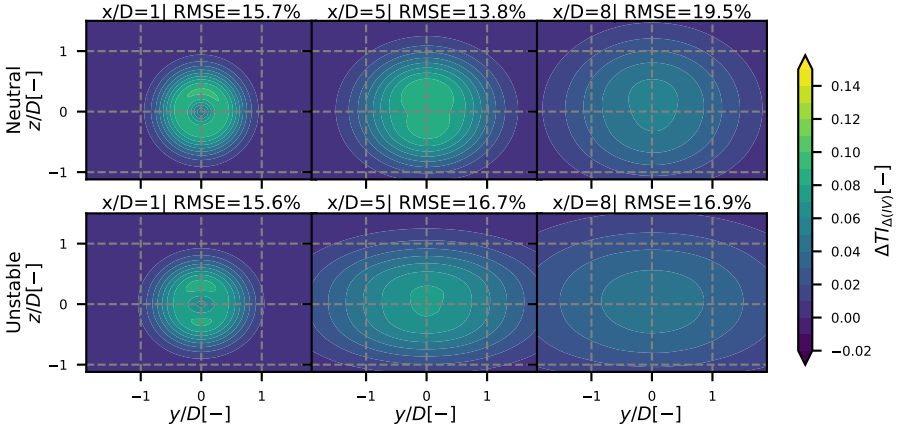

Figure 12. Results of $\Delta k_{x,a,am}$ i.e. the model for term Δ(IV) for the neutral and unstable cases. The RMSE is given with respect to the term $\Delta k_{x,a}$ computed from Meso-NH (Fig. 11).

It can be noted that in absence of meandering, i.e. for $\sigma_f = 0$, the model retrieves its MFOR form (Eq. 19). The result of Eq. 32 is plotted in Fig. 12 at three positions downstream in the neutral and unstable cases, and the RMSE is given with

respect to the LESs results for term Δk_a (Fig. 11). As for the term (I) and (III), the expression of $k_{a,am}$ is based on a Gaussian velocity deficit hypothesis, even in the near wake where the LES wake ~~is~~ takes a shape closer to a top-hat function. The velocity gradient that is the source of the rotor-added turbulence is thus lower and more spread in the model compared to the actual values. Another issue of the model is that it poorly takes into account shear, due to the assumptions of Eqs. 18 and 23. Indeed, the only source of vertical asymmetry in Eq. 32 is U_∞^2, i.e. the velocity shear upstream of the turbine. In the neutral case, it leads to a model that is less asymmetric than what is observed in the MFOR in Meso-NH (Fig. 3), and this error propagates in the FFOR. In the unstable case, this issue is less marked due to weaker shear upstream of the turbine.

5.3 Results of the model for turbulence

For the turbulence, a model is found only for terms (III) (Eq. 28) and Δ(IV) (Eq. 32). Even though the contribution of the three cross-terms of Eq. 7 is not negligible, the two modelled terms are ~~the main contributions~~ predominant and the result of the model limited to these two terms can be compared to the turbulence in the FFOR. The total modelled turbulence is here computed as:

$$k_{x,am} = k_\infty + k_{x,m,am} + \Delta k_{x,a,am}. \tag{34}$$

where k_∞ is taken directly 2.5 D upstream of the turbine in the LESs datasets. With the same plotting convention as in Figs. 7 and 8, the profiles of turbulence in the horizontal and vertical directions are plotted in Figs. 13 and 14 for the neutral and unstable cases, respectively.

As it has been noted in Sects. 5.1 and 5.2, the error on the near-wake velocity model due to the Gaussian shape assumption propagates on the turbulence model. More realistic shapes (~~double~~ double- or super-Gaussian) that show larger wake-generated shear in the near wake would result in higher and more localised meandering and rotor-added turbulence, as in the Meso-NH profiles. At $x/D = 5$ and $x/D = 8$ i.e. when the Gaussian velocity shape is reached, the results of the model in both cases are much better, in particular in the horizontal direction: the order of magnitude is respected and the positions of maxima are correct. In the neutral case, where a double peak shape is still distinguishable at these positions, the minimum of turbulence located at $y = 0$ is slightly overestimated.

The vertical profiles (bottom lines of Figs. 13 and 14) show less good results. In the neutral case, in particular, the maxima of the double Gaussian shape are ~~situated~~ located near $z/D \pm 0.3$ instead of the tip positions $z/D \pm 0.5$ as seen in the LESs data. Moreover, the turbulence is overestimated in the bottom part of the wake and underestimated in the top part. This is the combination of two different issues. On one hand, the terms (V) and (VI) from Eq. 7 are not modelled yet and it has been shown in the companion paper that these terms (in particular the term (V)) redistribute the TKE from the bottom to the top of the wake. The error due to this first approximation is represented by the difference between the blue and black curves. On the other hand, the shear in the model is only accounted for through U_∞^2 in factor of $k_{m,am}$ and $k_{a,am}$. This small contribution is compensated by the upstream turbulence k_∞ that is larger at the bottom than at the top, leading to ~~an~~ almost symmetric vertical

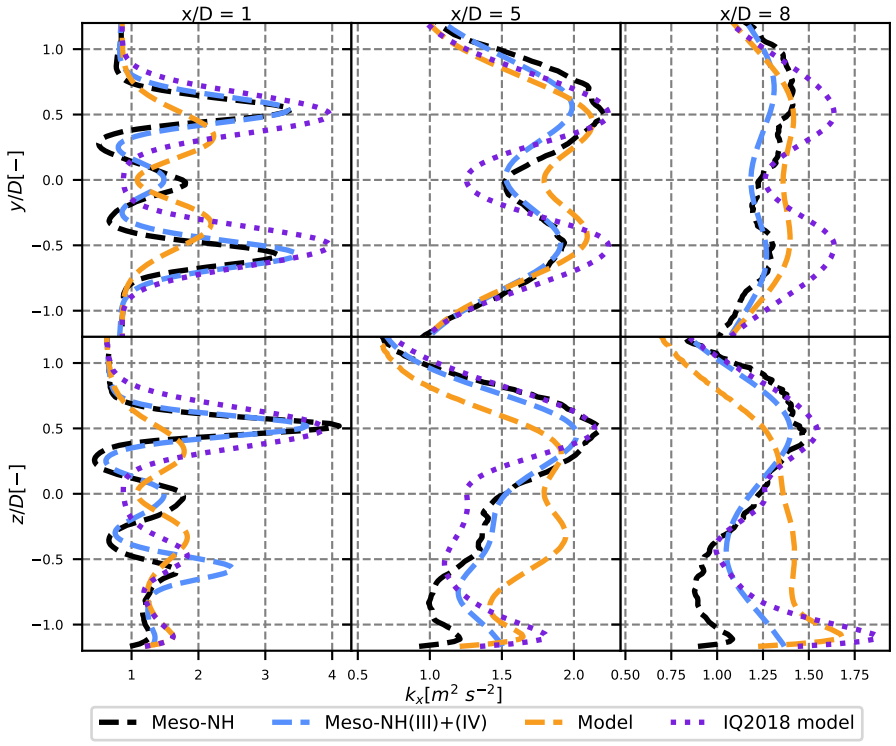

Figure 13. Results of the axial turbulence analytical velocity model (orange) in the neutral case, compared to the modelled terms in Meso-NH (blue) and the total turbulence in the FFOR (black). Lateral (top) and vertical (bottom) profiles are plotted for different positions downstream. The IQ2018 model is plotted in purple for comparison.

profiles for the model ~~profiles~~ whereas the LES profiles, even when neglecting the cross-terms, have much stronger asymmetry. The error due to this second approximation is represented by the difference between the orange and blue curves.

In ~~the~~ purple is also plotted the model of Ishihara and Qian (2018), denoted IQ2018 hereafter. The results from IQ2018 are obtained from the values of C_T, TI_x and k_x upstream of the turbine (see Sect. 2). It should be noted that the comparison is not very fair because our model has not been calibrated and thus does not depend on calibration like IQ2018. We can note that the IQ2018 model gives fairly good results for vertical profiles, due to the correction near the ground proposed by the authors. However, for the IQ2018 profile to show a peak at the top tip, it needs to also show a double peak for the y profile (see Fig. 13 at x/D=8), a phenomenon that is not observed in the LES and that is not necessarily seen in our model due to the definition of σ and σ_f in the two directions

In the unstable case, the results of ~~the~~ our model are surprisingly better than the Meso-NH approximation of (III)+(IV) near the ground. A possible explanation would be that in the unstable case, the meandering standard deviation σ_f becomes larger than the wake width in the MFOR σ (see Fig. 6), and that both $k_{m,am}$ and $k_{a,am}$ tends toward a Gaussian shape in these

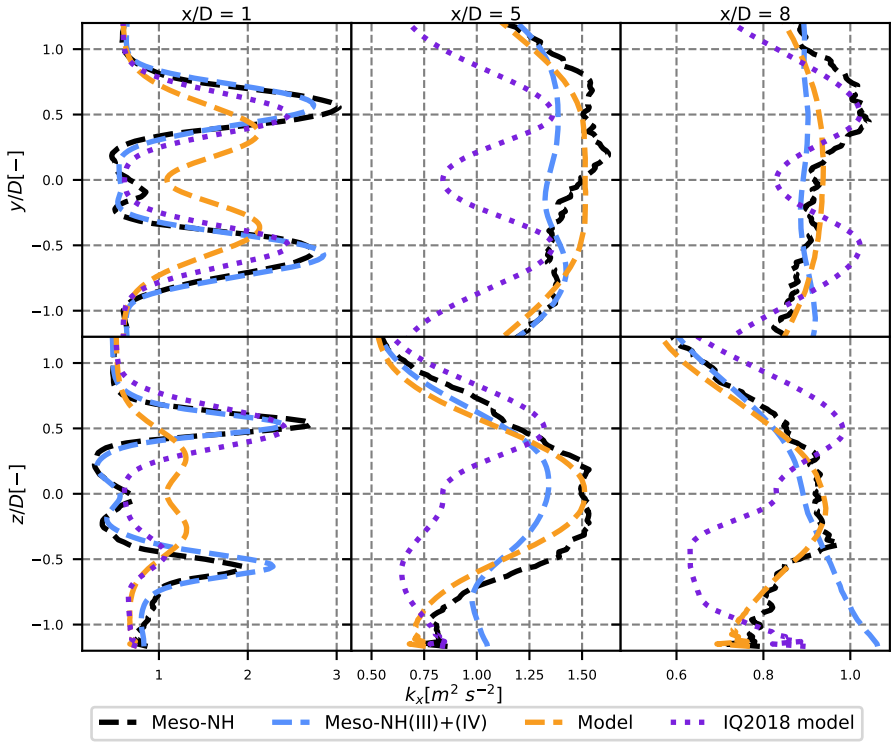

Figure 14. Results of the axial turbulence analytical velocity model (orange) in the unstable case, compared to the modelled terms in Meso-NH (blue) and the total turbulence in the FFOR (black). Lateral (top) and vertical (bottom) profiles are plotted for different positions downstream. The IQ2018 model is plotted in purple for comparison.

conditions. Consequently, and despite the error induced by neglecting terms (V) and (VI), it is not surprising to find a vaguely Gaussian function in the modelled unstable case, which happens to be the actual shape of the turbulence field.

The unstable case shows the main shortcoming of the IQ2018 model and the added value of our model. Besides the upstream turbulence profiles, the inflow conditions used in the IQ2018 are very similar between the neutral and unstable cases. Consequently, the purple profiles are alike in Figs. 13 and 14 whereas the stronger meandering in the unstable case leads to a Gaussian-like turbulence profile, even in the vertical direction. The maximum turbulence is thus no longer located at the top tip but rather at hub height. This property is well-predicted by our model whereas the IQ2018 model, which does not take meandering into account, predicts quasi-identical behaviours between the neutral and unstable cases.

6 Conclusions and perspectives

This work is the second part of a ~~two steps study that aimed~~ two-step study that aims at modelling the turbulence in the wake of a wind turbine based on the meandering phenomenon. In the companion paper, the velocity and turbulence in the FFOR

were broken down into different terms, ~~and~~ some of which have been shown to be negligible. In the present work, an analytical model is proposed for the dominating terms of the turbulence breakdown, i.e. the meandering turbulence and the rotor-added turbulence. The originality of this work is that it allows calibrating independently the effects of meandering and of the wake expansion ~~,~~ and that it gives the whole turbulence profile rather than only the maximum value. For the velocity, it writes:

$$U_{am}(y,z) = U_\infty(z)\left(1 + C\sqrt{\frac{\sigma_y^2}{\sigma_y^2+\sigma_{fy}^2}\frac{\sigma_z^2}{\sigma_z^2+\sigma_{fz}^2}}\exp\left(-\frac{y^2}{2\sigma_y^2+2\sigma_{fy}^2}-\frac{z^2}{2\sigma_z^2+2\sigma_{fz}^2}\right)\right) \tag{35}$$

and for the turbulence:

$$\begin{aligned} k_{am} = k_\infty + \\ (CU_\infty(z))^2\left[\sqrt{\frac{\sigma_y^2}{\sigma_y^2+2\sigma_{fy}^2}}\sqrt{\frac{\sigma_z^2}{\sigma_z^2+2\sigma_{fz}^2}}\exp\left(-\frac{y^2}{\sigma_y^2+2\sigma_{fy}^2}-\frac{z^2}{\sigma_z^2+2\sigma_{fz}^2}\right)-\frac{\sigma_y^2}{\sigma_y^2+\sigma_{fy}^2}\frac{\sigma_z^2}{\sigma_z^2+\sigma_{fz}^2}\exp\left(-\frac{y^2}{\sigma_y^2+\sigma_{fy}^2}-\frac{z^2}{\sigma_z^2+\sigma_{fz}^2}\right)\right]+ \\ \frac{\left(CU_\infty(z)l_m(x)\right)^2/\left(2C_\mu^{1/2}\right)}{\sqrt{1+2(\sigma_{fy}/\sigma_y)^2}\sqrt{1+2(\sigma_{fz}/\sigma_z)^2}}\left(\frac{y^2\sigma_y^2+\sigma_y^2\sigma_{fy}^2+2\sigma_{fy}^4}{\sigma_y^2(\sigma_y^2+2\sigma_{fy}^2)^2}+\frac{z^2\sigma_z^2+\sigma_z^2\sigma_{fz}^2+2\sigma_{fz}^4}{\sigma_z^2(\sigma_z^2+2\sigma_{fz}^2)^2}\right)\exp\left(-\frac{y^2}{\sigma_y^2+2\sigma_{fy}^2}-\frac{z^2}{\sigma_z^2+2\sigma_{fz}^2}\right) \end{aligned} \tag{36}$$

where $C = 1-\sqrt{1-C_T/(8\sigma_y\sigma_z/D^2)}$, C_T is the thrust coefficient, D is the turbine diameter, k_∞ and U_∞ are the upstream turbulence and velocities and C_μ is a constant. The model's parameters are the wake widths σ_y, σ_z, the amount of meandering σ_{fy}, σ_{fz} and the mixing length l_m. The expressions of velocity and added turbulence in the MFOR ~~that are~~ used to build Eqs. 35 and 36 can also be used as inputs to the DWM: combined with a synthetic turbulence generation, the unsteady effects of meandering can be modelled.

The model has been tested on two LESs datasets that simulated a single wind turbine wake under a neutral and an unstable atmosphere. For the velocity, the results are satisfactory, either in the vertical or lateral direction. The horizontal turbulence profiles are also satisfying but in the vertical direction, due to the neglected terms and to a very simple treatment of shear, the model is overestimating turbulence at the bottom of the wake and underestimating it at the top. This lack of asymmetry is attributed to the simplifications made on the atmospheric shear and to the absence of the covariance term that redistributes vertically the turbulence in the model.

This is the first step toward a fully analytical, physically-based model for turbulence and velocity in the wake of a wind turbine. For future works, it would be interesting to derive an analytical model for the other terms of the turbulence breakdown. As shown in Figs. 7, 8, 13 and 14 the error induced by neglecting cross-terms (between black and blue curves) is lower than the error of the model itself (between blue and orange curves) but modelling these terms could improve the results, in particular in the vertical direction. The treatment of shear must be improved to model more realistically vertical turbulence profiles. The added turbulence in the MFOR could also be improved by taking into account the velocity gradient in the streamwise direction $\partial U_x/\partial x$. For the model to be complete, an expression for every term of the Reynolds-stress tensor (or at least the diagonal

terms to get the total TKE) would be needed, which implies a model for the lateral and vertical velocities U_y and U_z. A better ~~near wake~~ near-wake modelling could be achieved by using a non-Gaussian velocity assumption in the vicinity of the rotor (such as super-Gaussian or double-Gaussian functions). Taking into account veer such as in Abkar et al. (2018) is necessary to apply the model to cases where the wake is skewed, typically in cases of a stably stratified ABL. Finally, a calibration (i.e. relating different parameters σ, σ_f and l_m to the inflow conditions) under different atmospheric conditions will be needed to have an operational method.

Code and data availability. The code Meso-NH is open-source and can be downloaded on the dedicated website. The authors can provide the source code of the modified version 5-4-3 that was used in this work. The data used for the plot presented here and in part 1 are available under this online deposit: 10.5281/zenodo.6562720. The model equations have been written in python under the following online deposit 10.5281/zenodo.6560685.

Author contributions. EJ wrote the analytical model with FB. All the authors worked on the interpretation of the results. The manuscript has been written by EJ with the feedbacks of FB and VM.

Competing interests. The authors declare that they have no competing interests.

References

Abkar, M. and Porté-Agel, F.: Influence of atmospheric stability on wind-turbine wakes: A large-eddy simulation study, Physics of Fluids, 27, 035 104, https://doi.org/10.1063/1.4913695, 2015.

Abkar, M., Sørensen, J., and Porté-Agel, F.: An Analytical Model for the Effect of Vertical Wind Veer on Wind Turbine Wakes, Energies, 11, 1838, https://doi.org/10.3390/en11071838, 2018.

Bastankhah, M. and Porté-Agel, F.: A new analytical model for wind-turbine wakes, Renewable Energy, 70, 116–123, https://doi.org/10.1016/j.renene.2014.01.002, 2014.

Blondel, F. and Cathelain, M.: An alternative form of the super-Gaussian wind turbine wake model, https://doi.org/10.5194/wes-2019-99, 2020.

Braunbehrens, R. and Segalini, A.: A statistical model for wake meandering behind wind turbines, Journal of Wind Engineering and Industrial Aerodynamics, 193, 103 954, https://doi.org/10.1016/j.jweia.2019.103954, 2019.

Brugger, P., Markfort, C., and Porté-Agel, F.: Field measurements of wake meandering at a utility-scale wind turbine with nacelle-mounted Doppler lidars, Wind Energy Science, 7, 185–199, https://doi.org/10.5194/wes-7-185-2022, 2022.

Conti, D., Dimitrov, N., Peña, A., and Herges, T.: Probabilistic estimation of the Dynamic Wake Meandering model parameters using SpinnerLidar-derived wake characteristics, Wind Energy Science, 6, 1117–1142, https://doi.org/10.5194/wes-6-1117-2021, 2021.

Crespo, A. and Hernandez, J.: Turbulence characteristics in wind-turbine wakes, Journal of Wind Engineering and Industrial Aerodynamics, 61, 71–85, https://doi.org/10.1016/0167-6105(95)00033-x, 1996.

Du, B., Ge, M., Zeng, C., Cui, G., and Liu, Y.: Influence of atmospheric stability on wind turbine wakes with a certain hub-height turbulence intensity, Physics of Fluids, https://doi.org/10.1063/5.0050861, 2021.

Frandsen, S.: Turbulence and turbulence-generated structural loading in wind turbine clusters, Ph.D. thesis, DTU, risø-R-1188(EN), 2007.

Frandsen, S., Barthelmie, R., Pryor, S., Rathmann, O., Larsen, S., Højstrup, J., and Thøgersen, M.: Analytical modelling of wind speed deficit in large offshore wind farms, Wind Energy, 9, 39–53, https://doi.org/10.1002/we.189, 2006.

Fuertes, F. C., Markfort, C., and Porté-Agel, F.: Wind Turbine Wake Characterization with Nacelle-Mounted Wind Lidars for Analytical Wake Model Validation, Remote Sensing, 10, 668, https://doi.org/10.3390/rs10050668, 2018.

Ishihara, T. and Qian, G.-W.: A new Gaussian-based analytical wake model for wind turbines considering ambient turbulence intensities and thrust coefficient effects, Journal of Wind Engineering and Industrial Aerodynamics, 177, 275–292, https://doi.org/10.1016/j.jweia.2018.04.010, 2018.

Iungo, G. V., Santhanagopalan, V., Ciri, U., Viola, F., Zhan, L., Rotea, M. A., and Leonardi, S.: Parabolic RANS solver for low-computational-cost simulations of wind turbine wakes, Wind Energy, 21, 184–197, https://doi.org/10.1002/we.2154, 2017.

Jensen, N.: A note on wind turbine interaction, techreport, Risoe National Laboratory, 1983.

Jézéquel, E., Cathelain, M., Masson, V., and Blondel, F.: Validation of wind turbine wakes modelled by the Meso-NH LES solver under different cases of stability, J Phys : Conf Ser, 1934, 012 003, https://doi.org/10.1088/1742-6596/1934/1/012003, 2021.

Jézéquel, E., Blondel, F., and Masson, V.: Analysis of wake properties and meandering under different cases of atmospheric stability: a large eddy simulation study, Journal of Physics: Conference Series, 2265, 022 067, https://doi.org/10.1088/1742-6596/2265/2/022067, 2022.

Keane, A., Aguirre, P. E. O., Ferchland, H., Clive, P., and Gallacher, D.: An analytical model for a full wind turbine wake, J Phys : Conf Ser, 753, 032 039, https://doi.org/10.1088/1742-6596/753/3/032039, 2016.

Keck, R.-E., Veldkamp, D., Madsen, H. A., and Larsen, G.: Implementation of a Mixing Length Turbulence Formulation Into the Dynamic Wake Meandering Model, Journal of Solar Energy Engineering, 134, https://doi.org/10.1115/1.4006038, 2012.

Keck, R.-E., Maré, M. d., Churchfield, M. J., Lee, S., Larsen, G., and Madsen, H. A.: Two improvements to the dynamic wake meandering model: including the effects of atmospheric shear on wake turbulence and incorporating turbulence build-up in a row of wind turbines, Wind Energy, pp. n/a–n/a, https://doi.org/10.1002/we.1686, 2013.

Lac, C., Chaboureau, J.-P., Masson, V., Pinty, J.-P., Tulet, P., Escobar, J., Leriche, M., Barthe, C., Aouizerats, B., Augros, C., Aumond, P., Auguste, F., Bechtold, P., Berthet, S., Bielli, S., Bosseur, F., Caumont, O., Cohard, J.-M., Colin, J., Couvreux, F., Cuxart, J., Delautier, G., Dauhut, T., Ducrocq, V., Filippi, J.-B., Gazen, D., Geoffroy, O., Gheusi, F., Honnert, R., Lafore, J.-P., Brossier, C. L., Libois, Q., Lunet, T., Mari, C., Maric, T., Mascart, P., Mogé, M., Molinié, G., Nuissier, O., Pantillon, F., Peyrillé, P., Pergaud, J., Perraud, E., Pianezze, J., Redelsperger, J.-L., Ricard, D., Richard, E., Riette, S., Rodier, Q., Schoetter, R., Seyfried, L., Stein, J., Suhre, K., Taufour, M., Thouron, O., Turner, S., Verrelle, A., Vié, B., Visentin, F., Vionnet, V., and Wautelet, P.: Overview of the Meso-NH model version 5.4 and its applications, Geoscientific Model Development, 11, 1929–1969, https://doi.org/10.5194/gmd-11-1929-2018, 2018.

Larsen, G. C., Madsen, H. A., Thomsen, K., and Larsen, T. J.: Wake meandering: a pragmatic approach, Wind Energy, 11, 377–395, https://doi.org/10.1002/we.267, 2008.

Madsen, H. A., Larsen, G. C., Larsen, T. J., Troldborg, N., and Mikkelsen, R.: Calibration and Validation of the Dynamic Wake Meandering Model for Implementation in an Aeroelastic Code, Journal of Solar Energy Engineering, 132, https://doi.org/10.1115/1.4002555, 2010.

Niayifar, A. and Porté-Agel, F.: Analytical Modeling of Wind Farms:A New Approach for Power Prediction, Energies, 2016.

Pope, S. B.: Turbulent Flows, Cambridge University Press, https://doi.org/10.1017/cbo9780511840531, 2000.

Scherfgen, D.: Integral Calculator., https://www.integral-calculator.com/, accessed: 2022-04-29.

Stein, V. P. and Kaltenbach, H.-J.: Non-Equilibrium Scaling Applied to the Wake Evolution of a Model Scale Wind Turbine, Energies, 12, 2763, https://doi.org/10.3390/en12142763, 2019.

Teitelbaum, J.: Convolution of Gaussians is Gaussian., https://jeremy9959.net/Math-5800-Spring-2020/notebooks/convolution_of_gaussians.html, accessed: 2022-04-29.

Xie, S. and Archer, C.: Self-similarity and turbulence characteristics of wind turbine wakes via large-eddy simulation, Wind Energy, 18, 1815–1838, https://doi.org/10.1002/we.1792, 2014.